LETTER

doi:10.1038/nature14340

An ultrafast rechargeable aluminium-ion battery

Meng-Chang Lin[1,2]*, Ming Gong[1]*, Bingan Lu[1,3]*, Yingpeng Wu[1]*, Di-Yan Wang[1,4,5], Mingyun Guan[1], Michael Angell[1], Changxin Chen[1], Jiang Yang[1], Bing-Joe Hwang[6] & Hongjie Dai[1]

The development of new rechargeable battery systems could fuel various energy applications, from personal electronics to grid storage[1,2]. Rechargeable aluminium-based batteries offer the possibilities of low cost and low flammability, together with three-electron-redox properties leading to high capacity[3]. However, research efforts over the past 30 years have encountered numerous problems, such as cathode material disintegration[4], low cell discharge voltage (about 0.55 volts; ref. 5), capacitive behaviour without discharge voltage plateaus (1.1–0.2 volts[6] or 1.8–0.8 volts[7]) and insufficient cycle life (less than 100 cycles) with rapid capacity decay (by 26–85 per cent over 100 cycles)[4–7]. Here we present a rechargeable aluminium battery with high-rate capability that uses an aluminium metal anode and a three-dimensional graphitic-foam cathode. The battery operates through the electrochemical deposition and dissolution of aluminium at the anode, and intercalation/de-intercalation of chloroaluminate anions in the graphite, using a non-flammable ionic liquid electrolyte. The cell exhibits well-defined discharge voltage plateaus near 2 volts, a specific capacity of about 70 mA h g^{-1} and a Coulombic efficiency of approximately 98 per cent. The cathode was found to enable fast anion diffusion and intercalation, affording charging times of around one minute with a current density of ~4,000 mA g^{-1} (equivalent to ~3,000 W kg^{-1}), and to withstand more than 7,500 cycles without capacity decay.

Owing to the low-cost, low-flammability and three-electron redox properties of aluminium (Al), rechargeable Al-based batteries could in principle offer cost-effectiveness, high capacity and safety, which would lead to a substantial advance in energy storage technology[3,8]. However, research into rechargeable Al batteries over the past 30 years has failed to compete with research in other battery systems. This has been due to problems such as cathode material disintegration[4], low cell discharge voltage (~0.55 V; ref. 5), capacitive behaviour without discharge voltage plateaus (1.1–0.2 V, or 1.8–0.8 V; refs 6 and 7, respectively), and insufficient cycle life (<100 cycles) with rapid capacity decay (by 26–85% over 100 cycles)[4–7]. Here we report novel graphitic cathode materials that afford unprecedented discharge voltage profiles, cycling stabilities and rate capabilities for Al batteries.

We constructed Al/graphite cells (see diagram in Fig. 1a) in Swagelok or pouch cells, using an aluminium foil (thickness ~15–250 μm) anode, a graphitic cathode, and an ionic liquid electrolyte made from vacuum dried $AlCl_3$/1-ethyl-3-methylimidazolium chloride ([EMIm]Cl; see Methods, residual water ~500 p.p.m.). The cathode was made from either pyrolytic graphite (PG) foil (~17 μm) or a three-dimensional graphitic foam[9,10]. Both the PG foil and the graphitic-foam materials exhibited typical graphite structure, with a sharp (002) X-ray diffraction (XRD) graphite peak at $2\theta \approx 26.55^\circ$ (d spacing, 3.35 Å; Extended Data Fig. 1). The cell was first optimized in a Swagelok cell operating at 25 °C with a PG foil cathode. The optimal ratio of $AlCl_3$/[EMIm]Cl was found to be ~1.3–1.5 (Extended Data Fig. 2a), affording a specific discharging capacity of 60–66 mA h g^{-1} (based on graphitic cathode mass) with a Coulombic efficiency of 95–98%. Raman spectroscopy revealed that with an $AlCl_3$/[EMIm]Cl ratio of ~1.3, both $AlCl_4^-$ and $Al_2Cl_7^-$ anions were present (Extended Data Fig. 2b) at a ratio $[AlCl_4^-]/[Al_2Cl_7^-] \approx 2.33$

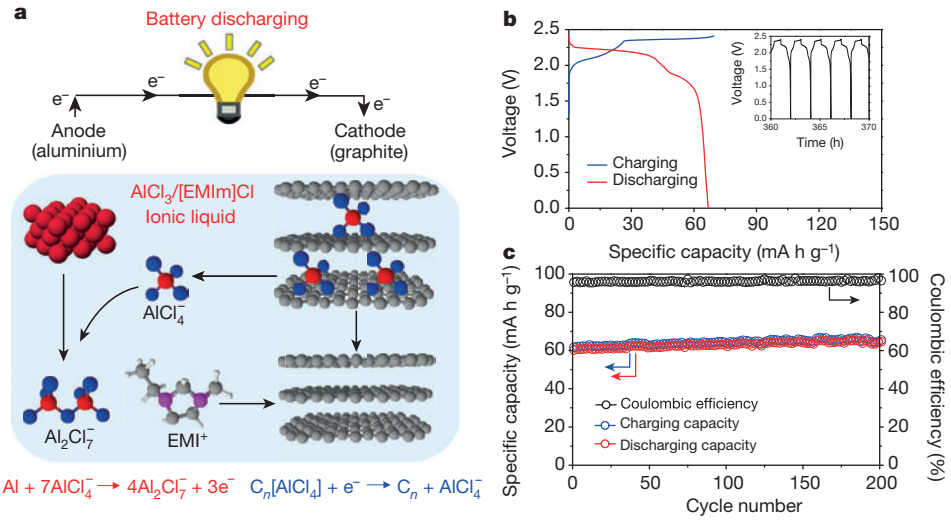

Figure 1 | Rechargeable Al/graphite cell. **a**, Schematic drawing of the Al/graphite cell during discharge, using the optimal composition of the $AlCl_3$/[EMIm]Cl ionic liquid electrolyte. On the anode side, metallic Al and $AlCl_4^-$ were transformed into $Al_2Cl_7^-$ during discharging, and the reverse reaction took place during charging. On the cathode side, predominantly $AlCl_4^-$ was intercalated and de-intercalated between graphite layers during charge and discharge reactions, respectively. **b**, Galvanostatic charge and discharge curves of an Al/pyrolytic graphite (PG) Swagelok cell at a current density of 66 mA g^{-1}. Inset, charge and discharge cycles. **c**, Long-term stability test of an Al/PG cell at 66 mA g^{-1}.

[1]Department of Chemistry, Stanford University, Stanford, California 94305, USA. [2]Green Energy and Environment Research Laboratories, Industrial Technology Research Institute, Hsinchu 31040, Taiwan. [3]School of Physics and Electronics, Hunan University, Changsha 410082, China. [4]Department of Chemistry, National Taiwan Normal University, Taipei 11677, Taiwan. [5]Institute of Atomic and Molecular Sciences, Academia Sinica, Taipei 10617, Taiwan. [6]Department of Chemical Engineering, National Taiwan University of Science and Technology, Taipei 10607, Taiwan.
*These authors contributed equally to this work.

(ref. 11). The cathode specific discharging capacity was found to be independent of graphite mass (Extended Data Fig. 3), suggesting that the entirety of the graphite foil participated in the cathode reaction.

The Al/PG cell exhibited clear discharge voltage plateaus in the ranges 2.25–2.0 V and 1.9–1.5 V (Fig. 1b). The relatively high discharge voltage plateaus are unprecedented among all past Al-ion charge-storage systems[4–7]. Similar cell operation was observed with the amount of electrolyte lowered to ~0.02 ml per mg of cathode material (Extended Data Fig. 4). Charge–discharge cycling at a current density of 66 mA g^{-1} (1 C charging rate) demonstrated the high stability of the Al/PG cell, which nearly perfectly maintained its specific capacity over >200 cycles with a 98.1 ± 0.4% Coulombic efficiency (Fig. 1c). This was consistent with the high reversibility of Al dissolution/deposition, with Coulombic efficiencies of 98.6–99.8% in ionic liquid electrolytes[12–15]. No dendrite formation was observed on the Al electrode after cycling (Extended Data Fig. 5). To maintain a Coulombic efficiency >96%, the cut-off voltage of the Al/PG cell (that is, the voltage at which charging was stopped) was set at 2.45 V, above which reduced efficiencies were observed (see Extended Data Fig. 6a), probably due to side reactions (especially above ~2.6 V) involving the electrolyte, as probed by cyclic voltammetry with a glassy carbon electrode against Al (Extended Data Fig. 6b).

We observed lowered Coulombic efficiency and cycling stability of the Al/graphite cell when using electrolytes with higher water contents, up to ~7,500 p.p.m. (Extended data Fig. 6c, d), accompanied by obvious H_2 gas evolution measured by gas chromatography (Extended Data Fig. 6e). This suggested side reactions triggered by the presence of residual water in the electrolyte, with H_2 evolution under reducing potential on the Al side during charging. Further lowering the water content of the ionic liquid electrolyte could be important when maximizing the Coulombic efficiency of the Al/graphite cells.

The Al/PG cell showed limited rate capability with much lower specific capacity when charged and discharged at a rate higher than 1 C (Extended Data Fig. 7). It was determined that cathode reactions in the Al/PG cell involve intercalation and de-intercalation of relatively large chloroaluminate ($Al_xCl_y^-$) anions in the graphite (see below for XRD evidence of intercalation), and the rate capability is limited by slow diffusion of anions through the graphitic layers[16]. When PG was replaced by natural graphite, intercalation was evident during charging owing to dramatic expansion (~50-fold) of the cathode into loosely stacked flakes visible to the naked eye (Extended Data Fig. 8a). In contrast, expansion of PG foil upon charging the Al/PG cell was not observable by eye (Extended Data Fig. 8b), despite the similar specific charging capacity of the two materials (Extended Data Fig. 8c). This superior structural integrity of PG over natural graphite during charging was attributed to the existence of covalent bonding between adjacent graphene sheets in PG[17], which was not present in natural graphite. Using PG, which has an open, three-dimensionally-bound graphitic structure, we prevented excessive electrode expansion that would lead to electrode disintegration, while maintaining the efficient anion intercalation necessary for high performance.

Because high-rate and high-power batteries are highly desirable for applications such as electrical grid storage, the next step in the investigation was to develop a cathode material that would have reduced energetic barriers to intercalation during charging[16]. We investigated a flexible graphitic foam (Fig. 2a), which was made on a nickel foam template by chemical vapour deposition[9,10] (see Methods), as a possible material for

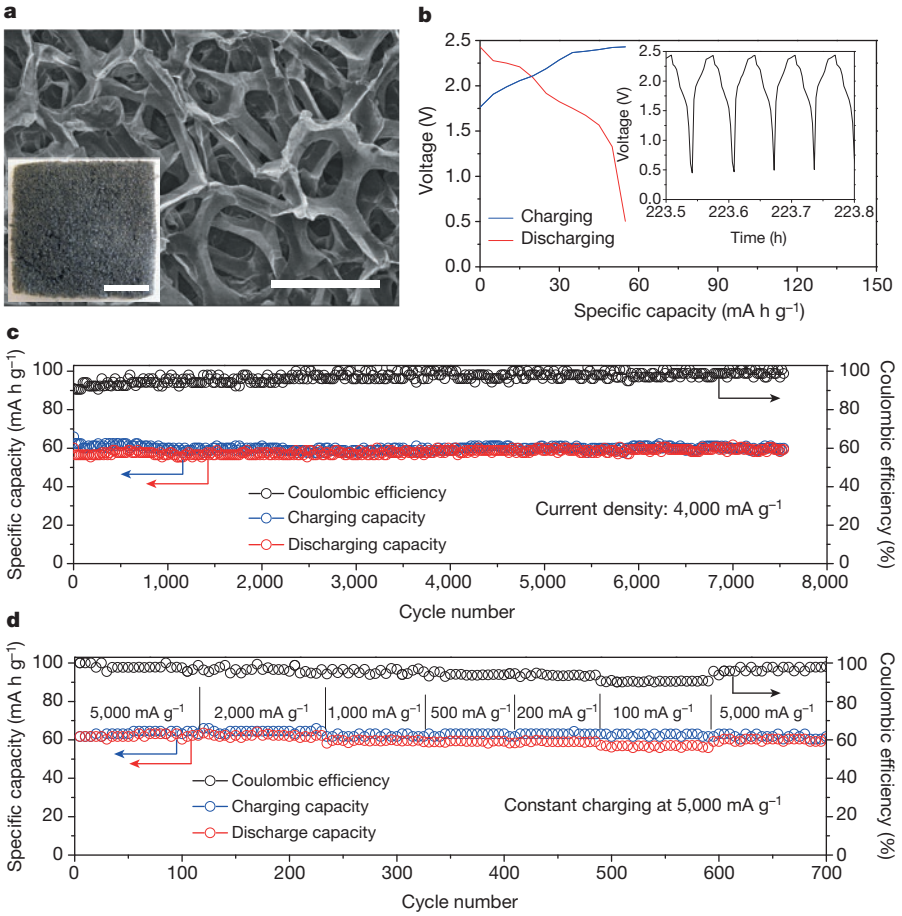

Figure 2 | An ultrafast and stable rechargeable Al/graphite cell. **a**, A scanning electron microscopy image showing a graphitic foam with an open frame structure; scale bar, 300 μm. Inset, photograph of graphitic foam; scale bar, 1 cm. **b**, Galvanostatic charge and discharge curves of an Al/graphitic-foam pouch cell at a current density of 4,000 mA g^{-1}. **c**, Long-term stability test of an Al/graphitic-foam pouch cell over 7,500 charging and discharging cycles at a current density of 4,000 mA g^{-1}. **d**, An Al/graphitic-foam pouch cell charging at 5,000 mA g^{-1} and discharging at current densities ranging from 100 to 5,000 mA g^{-1}.

ultrafast Al batteries. The graphite whiskers in the foam were 100 μm in width (Fig. 2a), with large spaces in between, which greatly decreased the diffusion length for the intercalating electrolyte anions and facilitated more rapid battery operation.

Remarkably, the Al/graphitic-foam cell (in a pouch cell configuration) could be charged and discharged at a current density up to 5,000 mA g^{-1}, about 75 times higher (that is, at a 75 C rate, <1 min charge/discharge time) than the Al/PG cell while maintaining a similar voltage profile and discharge capacity (~60 mA h g^{-1}) (Figs 1b and 2b). An impressive cycling stability with ~100% capacity retention was observed over 7,500 cycles with a Coulombic efficiency of 97 ± 2.3% (Fig. 2c). This is the first time an ultrafast Al-ion battery has been constructed with stability over thousands of cycles. The Al/graphitic-foam cell retained similar capacity and excellent cycling stability over a range of charge–discharge rates (1,000–6,000 mA g^{-1}) with 85−99% Coulombic efficiency (Extended Data Fig. 9a). It was also found that this cell could be rapidly charged (at 5,000 mA g^{-1}, in ~1 min) and gradually discharged (down to 100 mA g^{-1}, Fig. 2d and Extended Data Fig. 9b) over ~34 min while maintaining a high capacity (~60 mA h g^{-1}). Such a rapid charging/variable discharging rate could be appealing in many real-world applications.

We propose that simplified Al/graphite cell redox reactions during charging and discharging can be written as:

$$4Al_2Cl_7^- + 3e^- \rightleftharpoons Al + 7AlCl_4^- \quad (1)$$

$$C_n + AlCl_4^- \rightleftharpoons C_n[AlCl_4] + e^- \quad (2)$$

where n is the molar ratio of carbon atoms to intercalated anions in the graphite. The balanced $AlCl_4^-$ and $Al_2Cl_7^-$ concentrations in the electrolyte allowed for an optimal charging capacity at the cathode, with abundant $AlCl_4^-$ for charging/intercalation in graphite (equation (2)), and sufficient $Al_2Cl_7^-$ concentration for charging/electrodeposition at the anode (equation (1)).

Ex situ XRD measurement of graphite foil (Fig. 3a) confirmed graphite intercalation/de-intercalation by chloroaluminate anions during charging/discharging. The sharp pristine graphite foil (002) peak at $2\theta = 26.55°$ (d spacing = 3.35 Å) (Fig. 3a) vanished on charging to a specific capacity of ~30 mA h g^{-1}, while two new peaks appeared at ~28.25° ($d \approx 3.15$ Å) and ~23.56° ($d \approx 3.77$ Å) (Fig. 3a), with peak intensities further increasing on fully charging to ~62 mA h g^{-1}. The doublet XRD peak suggested highly strained graphene stacks formed on anion intercalation[18]. Analysis of the peak separation (see Methods) suggested a stage 4 graphite intercalation compound with an intercalant gallery height (spacing between adjacent graphitic host layers) of ~5.7 Å, indicating that the $AlCl_4^-$ anions (size ~5.28 Å; ref. 19) were intercalated between graphene layers in a distorted state. Full discharging led to the recovery of the graphite peak but with a broad shoulder (Fig. 3a), probably caused by irreversible changes in the stacking between the graphene layers or a small amount of trapped species.

In situ Raman spectroscopy was also performed to probe chloroaluminate anion intercalation/de-intercalation from graphite during cell charge/discharge (Fig. 3b). The graphite G band (~1,584 cm^{-1}) diminished and split into a doublet (1,587 cm^{-1} for the E_{2g2}(i) mode and ~1,608 cm^{-1} for the E_{2g2}(b) mode) upon anion intercalation (Fig. 3b)[20], and then evolved into a sharp new peak (~1,636 cm^{-1}, the G2 band of the E_{2g2}(b) mode, spectrum 2.41 V, Fig. 3b) once fully charged. The spectral changes were then reversed upon discharging (Fig. 3b), as the typical graphite Raman G band (1584 cm^{-1}) was recovered when fully discharged (spectrum 0.03 V, Fig. 3b). Similar Raman spectra and XRD data were obtained with a graphitic-foam cathode (Extended Data Fig. 10a, b). Interestingly, calcination of a fully charged PG foil at 850 °C in air (Fig. 3c) yielded a white aluminium oxide foam (Extended Data Fig. 10c), confirming the intercalation of chloroaluminate anions into the carbon network, which had been evidently removed oxidatively.

Lastly, X-ray photoelectron spectra (XPS) and Auger electron spectroscopy (AES) were performed to probe the chemical nature of the intercalated species in our graphitic cathodes (see Methods for details). To minimize the amount of trapped electrolyte, graphitic foam was used and the electrode was thoroughly washed with anhydrous methanol. XPS revealed that upon charging pristine graphite, the 284.8 eV C 1*s* peak developed a shoulder at higher energy (~285.9 eV, Fig. 4a), confirming electrochemical oxidation of graphitic carbon by intercalation of $AlCl_4^-$ anions (equation (2)). Chloroaluminate intercalation was evident from the appearance of Al 2*p* and Cl 2*p* peaks (Fig. 4b, c). Upon

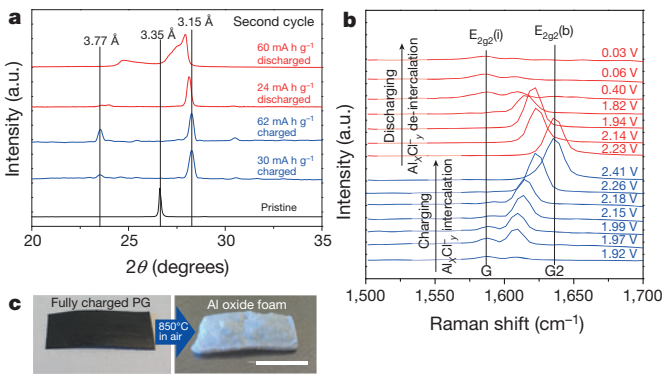

Figure 3 | Al/graphite cell reaction mechanisms. **a**, *Ex situ* X-ray diffraction patterns of PG in various charging and discharging states through the second cycle. **b**, *In situ* Raman spectra recorded for the PG cathode through a charge–discharge cycle, showing chloroaluminate anion intercalation/de-intercalation into graphite. **c**, After calcination of a fully charged (62 mA h g^{-1}) PG electrode at 850 °C in air, the sample completely transformed into a white foam made of aluminium oxide. Scale bar, 1 cm.

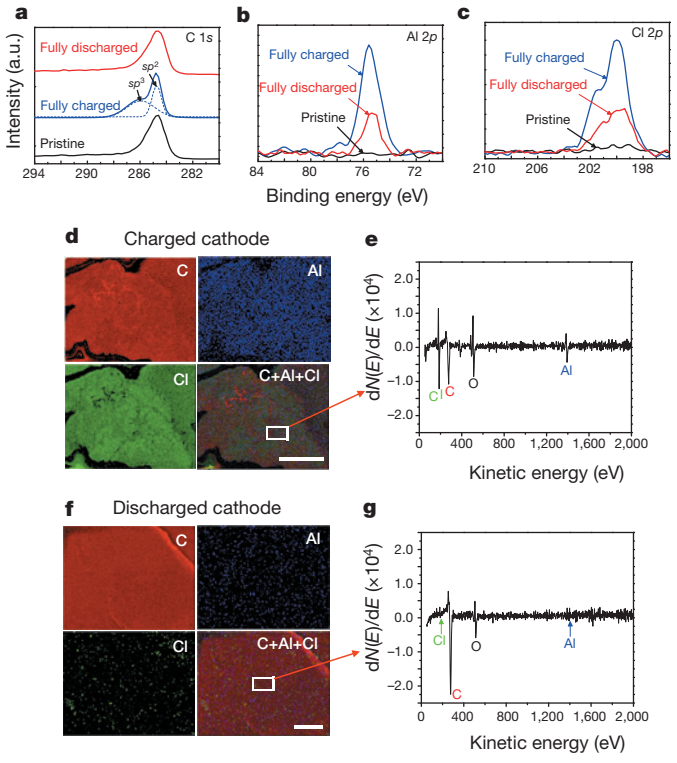

Figure 4 | Chemical probing of a graphitic cathode by XPS and AES. **a**, XPS data of the C 1*s* peak of a graphitic-foam electrode: pristine, fully charged and fully discharged. **b**, **c**, XPS data of Al 2*p* and Cl 2*p* peaks observed with a graphitic-foam electrode: pristine, fully charged and fully discharged. **d**–**g**, AES mapping images for C, Al and Cl (**d**, **f**), and the AES spectrum of the boxed regions (**e**, **g**) obtained with a fully charged graphitic-foam sample (**d**, **e**) and a fully discharged graphitic-foam sample (**f**, **g**). Scale bars: **d**, 25 μm; **f**, 10 μm.

discharging, the C 1*s* XPS spectrum of the cathode reverted to that of the pristine graphite due to anion de-intercalation and carbon reduction (Fig. 4a). Also, a substantial reduction in the Al 2*p* and Cl 2*p* signals was recorded over the graphite sample (see Fig. 4b, c). The remaining Al and Cl signals observed were attributed to trapped/adsorbed species in the graphite sample, which was probed by XPS over a large area. Furthermore, high spatial resolution AES elemental mapping of a single graphite whisker in the fully charged graphitic foam clearly revealed Al and Cl Auger signals uniformly distributed over the whisker (Fig. 4d, e), again confirming chloroaluminate anion intercalation. When fully discharged, AES mapping revealed anion de-intercalation from graphite with much lower Al and Cl Auger signals observed (Fig. 4f, g). These spectroscopic results clearly revealed chloroaluminate ion intercalation/de-intercalation in the graphite redox reactions involved in our rechargeable Al cell.

The Al battery pouch cell is mechanically bendable and foldable (Supplementary Video 1) owing to the flexibility of the electrode and separator materials. Further, we drilled through Al battery pouch cells during battery operation and observed no safety hazard, owing to the lack of flammability of the ionic liquid electrolyte in air (see Supplementary Video 2).

We have developed a new Al-ion battery using novel graphitic cathode materials with a stable cycling life up to 7,500 charge/discharge cycles without decay at ultrahigh current densities. The present Al/graphite battery can afford an energy density of $\sim$40 W h kg^{-1} (comparable to lead–acid and Ni–MH batteries, with room for improvement by optimizing the graphitic electrodes and by developing other novel cathode materials) and a high power density, up to 3,000 W kg^{-1} (similar to supercapacitors). We note that the energy/power densities were calculated on the basis of the measured $\sim$65 mA h g^{-1} cathode capacity and the mass of active materials in electrodes and electrolyte. Such rechargeable Al ion batteries have the potential to be cost effective and safe, and to have high power density.

Online Content Methods, along with any additional Extended Data display items and Source Data, are available in the online version of the paper; references unique to these sections appear only in the online paper.

Received 12 March 2014; accepted 6 February 2015.
Published online 6 April 2015.

1. Yang, Z. *et al.* Electrochemical energy storage for green grid. *Chem. Rev.* **111,** 3577–3613 (2011).
2. Huskinson, B. *et al.* A metal-free organic-inorganic aqueous flow battery. *Nature* **505,** 195–198 (2014).
3. Li, Q. & Bjerrum, N. J. Aluminum as anode for energy storage and conversion: a review. *J. Power Sources* **110,** 1–10 (2002).
4. Gifford, P. R. & Palmisano, J. B. An aluminum/chlorine rechargeable cell employing a room temperature molten salt electrolyte. *J. Electrochem. Soc.* **135,** 650–654 (1988).
5. Jayaprakash, N., Das, S. K. & Archer, L. A. The rechargeable aluminum-ion battery. *Chem. Commun.* **47,** 12610–12612 (2011).
6. Rani, J. V., Kanakaiah, V., Dadmal, T., Rao, M. S. & Bhavanarushi, S. Fluorinated natural graphite cathode for rechargeable ionic liquid based aluminum-ion battery. *J. Electrochem. Soc.* **160,** A1781–A1784 (2013).
7. Hudak, N. S. Chloroaluminate-doped conducting polymers as positive electrodes in rechargeable aluminum batteries. *J. Phys. Chem. C* **118,** 5203–5215 (2014).
8. Armand, M. & Tarascon, J. M. Building better batteries. *Nature* **451,** 652–657 (2008).
9. Yu, X., Lu, B. & Xu, Z. Super long-life supercapacitors based on the construction of nanohoneycomb-like strongly coupled $CoMoO_4$–3D graphene hybrid electrodes. *Adv. Mater.* **26,** 1044–1051 (2014).
10. Chen, Z. *et al.* Three-dimensional flexible and conductive interconnected graphene networks grown by chemical vapour deposition. *Nature Mater.* **10,** 424–428 (2011).
11. Wasserscheid, P. & Keim, W. Ionic liquids—new "solutions" for transition metal catalysis. *Angew. Chem. Int. Edn* **39,** 3772–3789 (2000).
12. Auborn, J. J. & Barberio, Y. L. An ambient temperature secondary aluminum electrode: its cycling rates and its cycling efficiencies. *J. Electrochem. Soc.* **132,** 598–601 (1985).
13. Wilkes, J. S., Levisky, J. A., Wilson, R. A. & Hussey, C. L. Dialkylimidazolium chloroaluminate melts: a new class of room-temperature ionic liquids for electrochemistry, spectroscopy and synthesis. *Inorg. Chem.* **21,** 1263–1264 (1982).
14. Lai, P. K. & Skyllas-Kazacos, M. Electrodeposition of aluminium in aluminium chloride/1-methyl-3-ethylimidazolium chloride. *J. Electroanal. Chem. Interfacial Electrochem.* **248,** 431–440 (1988).
15. Jiang, T., Chollier Brym, M. J., Dubé, G., Lasia, A. & Brisard, G. M. Electrodeposition of aluminium from ionic liquids: Part I—electrodeposition and surface morphology of aluminium from aluminium chloride ($AlCl_3$)–1-ethyl-3-methylimidazolium chloride ([EMIm]Cl) ionic liquids. *Surf. Coat. Tech.* **201,** 1–9 (2006).
16. Borg, R. J. & Dienes, G. J. *An Introduction to Solid State Diffusion* (Academic, 1988).
17. Zhu, Y.-J., Hansen, T. A., Ammermann, S., McBride, J. D. & Beebe, T. P. Nanometer-size monolayer and multilayer molecule corrals on HOPG: a depth-resolved mechanistic study by STM. *J. Phys. Chem. B* **105,** 7632–7638 (2001).
18. Schmuelling, G. *et al.* X-ray diffraction studies of the electrochemical intercalation of bis(trifluoromethanesulfonyl)imide anions into graphite for dual-ion cells. *J. Power Sources* **239,** 563–571 (2013).
19. Takahashi, S., Koura, N., Kohara, S., Saboungi, M. L. & Curtiss, L. A. Technological and scientific issues of room-temperature molten salts. *Plasmas Ions* **2,** 91–105 (1999).
20. Hardwick, L. J. *et al.* An *in situ* Raman study of the intercalation of supercapacitor-type electrolyte into microcrystalline graphite. *Electrochim. Acta* **52,** 675–680 (2006).

Supplementary Information is available in the online version of the paper.

Acknowledgements We thank M. D. Fayer for discussions. We also thank Y. Cui's group for use of an argon-filled glove box and a vacuum oven. M.-C.L thanks the Bureau of Energy, Ministry of Economic Affairs, Taiwan, for supporting international cooperation between Stanford University and ITRI. B.L. acknowledges support from the National Natural Science Foundation of China (grant no. 21303046), the China Scholarship Council (no. 201308430178), and the Hunan University Fund for Multidisciplinary Developing (no. 531107040762). We also acknowledge support from the US Department of Energy for novel carbon materials development and electrical characterization work (DOE DE-SC0008684), Stanford GCEP, the Precourt Institute of Energy, and the Global Networking Talent 3.0 plan (NTUST 104DI005) from the Ministry of Education of Taiwan.

Author Contributions M.-C.L., M.G., B.L. and Y.W. contributed equally to this work. M.-C.L. and H.D. conceived the idea for the project. B.L. prepared the graphitic foam. M.-C.L., M.G., B.L., Y.W., D.-Y.W., M.A. and M. Guan performed electrochemical experiments. M.-C.L., C.C. and J.Y conducted *in situ* Raman spectroscopy measurements. M.-C.L., M.G., B.L. and Y.W. performed *ex situ* X-ray diffraction measurements. M.G., M.-C.L., B.L. and Y.W. performed X-ray photoelectron spectroscopy and Auger electron spectroscopy measurements. M.-C.L., M.G., B.L., Y.W., D.-Y.W., M.A., B.-J.H. and H.D. discussed the results, analysed the data and drafted the manuscript.

Author Information Reprints and permissions information is available at www.nature.com/reprints. The authors declare no competing financial interests. Readers are welcome to comment on the online version of the paper. Correspondence and requests for materials should be addressed to H.D. (hdai@stanford.edu).

METHODS

Preparation of ionic liquid electrolytes. A room temperature ionic liquid electrolyte was made by mixing 1-ethyl-3-methylimidazolium chloride ([EMIm]Cl, 97%, Acros Chemicals) and anhydrous aluminium chloride ($AlCl_3$, 99.999%, Sigma Aldrich). [EMIm]Cl was baked at 130 °C under vacuum for 16–32 h to remove residual water. ([EMIm]Al_xCl_y) ionic liquid electrolytes were prepared in an argon-atmosphere glove box (both [EMIm]Cl and $AlCl_3$ are highly hygroscopic) by mixing anhydrous $AlCl_3$ with [EMIm]Cl, and the resulting light-yellow, transparent liquid was stirred at room temperature for 10 min. The mole ratio of $AlCl_3$ to [EMIm]Cl was varied from 1.1 to 1.8. The water content of the ionic liquid was determined (500–700 p.p.m.) using a coulometric Karl Fischer titrator, DL 39 (Mettler Toledo). The predominant anions in basic melts ($AlCl_3$/[EMIm]Cl mole ratio <1) are Cl^- and $AlCl_4^-$, while in acidic melts ($AlCl_3$/[EMIm]Cl mole ratio >1) chloroaluminate anions such as $Al_2Cl_7^-$, $Al_3Cl_{10}^-$, and $Al_4Cl_{13}^-$ are formed[11]. The ratio of anions to cations in the $AlCl_3$/[EMIm]Cl electrolyte was determined using a glass fibre filter paper (Whatman GF/D) loaded with a 4–8 μm Au-coated SiO_2 beads[21] in a cuvette cell (0.35 ml, Starna Cells) with random orientation quartz windows. Then, in the glove box, the cuvette cell was filled with $AlCl_3$/[EMIm]Cl = 1.3 (by mole). Raman spectra (200–650 cm^{-1}) were obtained using a 785-nm laser with 2 cm^{-1} resolution. Raman data were collected from the surface of the Au-coated SiO_2 bead so as to benefit from surface enhanced Raman[21,22] (Extended Data Fig. 2b).

Preparation of graphitic foam. Nickel (Ni) foams (Alantum Advanced Technology Materials, Shenyang, China), were used as 3D scaffold templates for the CVD growth of graphitic foam, following the process reported previously[9,10]. The Ni foams were heated to 1,000 °C in a horizontal tube furnace (Lindberg Blue M, TF55030C) under Ar (500 standard cubic centimetres per minute or s.c.c.m.) and H_2 (200 s.c.c.m.) and annealed for 10 min to clean their surfaces and to eliminate a thin surface oxide layer. Then, methane (CH_4) was introduced into the reaction tube at ambient pressure at a flow rate of 10 s.c.c.m., corresponding to a concentration of 1.4 vol.% in the total gas flow. After 10 min of reaction gas mixture flow, the samples were rapidly cooled to room temperature at a rate of 300 °C min^{-1} under Ar (500 s.c.c.m.) and H_2 (200 s.c.c.m.). The Ni foams covered with graphite were drop-coated with a poly(methyl methacrylate) (PMMA) solution (4.5% in ethyl acetate), and then baked at 110 °C for 0.5 h. The PMMA/graphene/Ni foam structure was obtained after solidification. Afterwards, these samples were put into a 3 M HCl solution for 3 h to completely dissolve the Ni foam to obtain the PMMA/graphite at 80 °C. Finally, the pure graphitic foam was obtained by removing PMMA in hot acetone at 55 °C and annealing in NH_3 (80 s.c.c.m.) at 600 °C for 2 h, and then annealing in air at 450 °C for 2 h. The microstructure of the graphitic foam was examined by SEM analysis using a FEI XL30 Sirion scanning electron microscope (Fig. 2a in the main text).

Preparation of glassy carbon. Glassy carbon (GC) was used as the current collector in the Swagelok-type cell. 72 g phenol (Sigma-Aldrich) and 4.5 ml ammonium hydroxide (30%, Fisher Scientific) were dissolved in 100 ml formaldehyde solution (37%, Fisher Scientific) under reflux while stirring rapidly. The solution was stirred at 90 °C until the solution turned a milk-white colour. Rotary evaporation was used to remove the water and get the phenolic resin. The phenolic resin was solidified at 100 °C in a mould (1/2-inch glass tube), and then carbonized at 850 °C under an Ar atmosphere for four hours to obtain the GC rod. The resulting GC rod contributed negligible capacity to the cathode (Extended Data Fig. 6b).

Electrochemical measurements. Prior to assembling the Al/graphite cell in the glove box, all components were heated under vacuum at 60 °C for more than 12 h to remove residual water. All electrochemical tests were performed at 25 ± 1 °C. A Swagelok-type cell (1/2 inch diameter) was constructed using a ~4 mg PG foil (0.017 mm, Suzhou Dasen Electronics Materials) cathode and a 90 mg Al foil (0.25 mm, Alfa Aesar) anode. A 1/2 inch GC rod (10 mm) was used as the current collector for the PG cathode, and a 1/2 inch graphite rod (10 mm) was used for the Al anode. Six layers of 1/2 inch glass fibre filter paper (Whatman 934-AH) were placed between the anode and cathode. Then, ~1.0 ml of ionic liquid electrolyte (prepared with $AlCl_3$/[EMIm]Cl mole ratios of 1.1, 1.3, 1.5 and 1.8) was injected and the cell sealed. The Al/PG cell was then charged (to 2.45 V) and discharged (to 0.01 V) at a current density of 66 mA g^{-1} with a MTI battery analyser (BST8-WA) to identify the ideal $AlCl_3$/[EMIm]Cl mole ratio (Extended Data Fig. 2a). To investigate the Coulombic efficiency of the Al/PG cell in $AlCl_3$/[EMIm]Cl ≈ 1.3 (by mole) electrolyte, the cell was charged to 2.45, 2.50, 2.55 and 2.60 V, respectively, and discharged to 0.4 V at a current density of 66 mA g^{-1} (Extended Data Fig. 6a). For long-term cycling stability tests, an Al/PG cell using electrolyte $AlCl_3$/[EMIm]Cl ≈ 1.3 by mole was charged/discharged at a current density of 66 mA g^{-1} (Fig. 1b, c in the main text). To study the rate capability of the Al/PG cell, the current densities were varied from 66 to 264 mA g^{-1} (Extended Data Fig. 7). Note that we lowered the electrolyte amount to ~0.02 ml per mg of cathode material and observed similar cell operation (Extended Data Fig. 4). Further decrease in the electrolyte ratio is possible through battery engineering.

PG foil was synthesized by pyrolysis of polyimide at high temperature, in which some covalent bonding is inevitably generated due to imperfections. Natural graphite foil was produced by compressing expanded graphite flakes, leading to stacking of natural graphite flakes by Van der Waals bonding between them. Similar battery characteristics were observed with PG and graphite foil electrodes, indicating that the battery behaviour was derived from the graphitic property of the electrodes (Extended Data Fig. 8c). However, since the natural graphite foils are synthesized by compressing expanded natural graphite powders without the covalent linkage between them, these foils suffered from drastic electrode expansion obvious to the naked eye, whereas pyrolytic graphite foils showed no obvious electrode expansion due to covalency (Extended Data Fig. 8a, b).

Pouch cells were assembled in the glove box using a graphitic-foam (~3 mg) cathode and an Al foil (~70 mg) anode, which were separated by two layers of glass fibre filter paper to prevent shorting. Polymer (0.1 mm × 4 mm × 5 mm) coated Ni foils (0.09 mm × 3 mm × 60 mm in size; MTI corporation) were used as current collectors for both anode and cathode. The electrolyte (~2 ml prepared using $AlCl_3$/[EMIm]Cl = 1.3 by mole) was injected and the cell was closed using a heat sealer. The cell was removed from the glove box for long-term cycling stability tests, in which the cell was charged/discharged at a current density of 4,000 mA g^{-1} (Fig. 2b, c). To determine the rate capability and fast-charge/slow-discharge behaviours of the Al/graphitic-foam cell, various current densities from 100 to 5,000 mA g^{-1} were used (Extended Data Fig. 9 and Fig. 2d). The pouch cell was charged to 2.42 V and discharged to a cut-off voltage of 0.5 V to prevent the dissolution reaction of Ni foil in the ionic liquid electrolyte.

Cyclic voltammetry measurements were performed using a potentiostat/galvanostat model CHI 760D (CH Instruments) in either three-electrode or two-electrode mode. The working electrode was an Al foil or a PG foil, the auxiliary electrode consisted of an Al foil, and an Al foil was used as the reference electrode. Copper tape (3M) was attached to these electrodes as the current collector. The copper tape was covered by poly-tetrafluoroethylene (PTFE) tape to prevent contact with the ionic liquid electrolyte and the part of the copper tape covered by PTFE was not immersed in the ionic liquid electrolyte. This prevented corrosion of the copper tape during cyclic voltammetry measurements. All three electrodes were placed in a plastic (1.5 ml) cuvette cell (containing electrolyte $AlCl_3$/[EMIm]Cl= 1.3 by mole) in the glove box, and then sealed with a rubber cap using a clamp. The scanning voltage range was set from –1.0 to 1.0 V (versus Al) for Al foil and 0 to 2.5 V (versus Al) for graphitic material, and the scan rate was 10 mV s^{-1} (Extended Data Fig. 10d). To investigate the working voltage range of the electrolyte without involving cathode intercalation, two-electrode measurement was performed by using a GC rod cathode against an Al anode in a Swagelok cell in $AlCl_3$/[EMIm]Cl (~1.3 by mole) electrolyte. The scanning voltage range was set from 0 to 2.9 V at a scan rate of 10 mV s^{-1} (Extended Data Fig. 6b).

We investigated the Al ion cell operation mechanism and electrode reactions in the ionic liquid electrolyte, using the optimal mole ratio of $AlCl_3$/[EMIm]Cl = 1.3. Using CV (Extended Data Fig. 10d), a reduction wave from –1.0 to –0.08 V (versus Al) and an oxidation wave from −0.08 to 0.80 V (versus Al) for the anode were observed (Extended Data Fig. 10d, left plot), corresponding to Al reduction/electrodeposition and oxidation/dissolution[13,15,23–25] during charging and discharging, respectively. This was consistent with Al redox electrochemistry in chloroaluminate ionic liquids[13,15,23–25] via equation (1) in the main text, and consistent with our Raman measurements, which showed both $AlCl_4^-$ and $Al_2Cl_7^-$ in the electrolyte (Extended Data Fig. 2b). On the graphitic cathode side, an oxidation wave of 1.83 to 2.50 V (versus Al) and a reduction wave of 1.16 to 2.36 V (versus Al) were observed (Extended Data Fig. 10d, right plot) and attributed to graphite oxidation and reduction through intercalation and de-intercalation of anions (predominantly $AlCl_4^-$ due to its smaller size), respectively. The oxidation voltage range of 1.83 to 2.50 V (versus Al, Extended Data Fig. 10d, right plot) was close to the anodic voltage range (1.8 to 2.2 V versus Al) of a previously reported dual-graphite cell[26] attributed to $AlCl_4^-$ intercalation in graphite. The reduction wave range of 1.16 to 2.36 V (versus Al) was assigned to the $AlCl_4^-$ de-intercalation[26]. The nature of the shoulder in the reduction curve of graphite ranging from 2.36 to 1.9 V (Extended Data Fig. 10d, right plot) and a higher discharge plateau (2.25 to 2.0 V) of an Al/PG cell upon charging (Fig. 1b in the main text) remained unclear, but could be due to different stages of anion–graphite intercalation[27].

XRD and Raman studies of graphite cathodes during charge and discharge. For *ex situ* X-ray diffraction (XRD) study, an Al/ PG cell (in a Swagelok configuration) was charged and discharged at a constant current density of 66 mA g^{-1}. The reactions were stopped after 30 mA h g^{-1} charged, fully charged (62 mA h g^{-1}) and 40 mA h g^{-1} discharged after charge/discharge capacities were in a stable state. Fully charged (62 mA h g^{-1}) graphitic foam was also prepared. After either the charge or the discharge reaction, the graphitic cathode was removed from the cell in the glove box. To avoid reaction between the cathode and air/moisture in the ambient atmosphere, the cathode was placed onto a glass slide and then wrapped in a Scotch tape.

The wrapped samples were immediately removed from the glove box for *ex situ* XRD measurements, which were performed on a PANalytical X'Pert instrument (Fig. 3a in the main text and Extended Data Fig. 10b).

The periodic repeat distance (I_C), the intercalant gallery height (d_i) and the gallery expansion (Δd)[28,29] can be calculated using

$$I_C = (d_i + 3.35\,\text{Å}) \times (n-1) = (\Delta d + 3.35\,\text{Å}) \times n = l \times d_{obs} \quad (3)$$

where l is the index of (00l) planes oriented in the stacking direction and d_{obs} is the observed value of the spacing between two adjacent planes[18,28,29]. The d spacing of graphite is 3.35 Å. During the charging/anion-intercalation process, the graphite (002) peak completely vanished and two new peaks arose. The intensity pattern is commonly found for a stage n graphite intercalation compound (GIC), where the most dominant peak is the $(00n+1)$ and the second most dominant peak is the $(00n+2)$[18,28,29]. Based on our experimental data, by increasing the charging state from 48–60% charged (30 mA h g^{-1}) to the fully charged state (62 mA h g^{-1}), the distance between the $(00n+1)$ and $(00n+2)$ peaks gradually increased, as more $Al_xCl_y^-$ anions intercalated. The d spacing values of $(00n+1)$ and $(00n+2)$ peaks (that is, $d_{(n+1)}$ and $d_{(n+2)}$, respectively) were calculated from XRD data (for example, Fig. 3a). By determining the ratio of the $d_{(n+2)}/d_{(n+1)}$ peak position and correlating these to the ratios of stage pure GICs (that is, ideal cases), the most dominant stage phase of the observed GIC can be assigned[28,29]. After assigning the (00l) indices, we calculated the intercalant gallery height (d_i) through equation (3).

For simultaneous *in situ* Raman and galvanostatic charge/discharge reaction measurements, a cuvette cell (0.35 ml, Starna Cells) with random orientation quartz windows was used. An aluminium foil and a graphitic material (PG or graphitic foam) were used as the anode and cathode, respectively. The electrolyte was mixed $AlCl_3$/[EMIm]Cl = 1.3 (by mole). The electrochemical cell was assembled in the glove box following the process mentioned above. Raman spectra were obtained (1,500–1,700 cm^{-1}) using a HeNe laser (633 nm) with 2 cm^{-1} resolution. The spectral data were collected after a few successive charge/discharge scans between 2.45 and 0.01 V at a current density of 66 mA g^{-1} (PG) (Fig. 3b in the main text) or 1,000 mA g^{-1} (graphitic foam) (Extended Data Fig. 10a).

XPS and AES measurements. Al/graphitic-foam cells were fully charged/discharged at a current density of 4,000 mA g^{-1}. Then, the Al/graphitic-foam cells were transferred to the glove box for preparation for XPS and AES analysis. Fully charged/discharged graphitic foams were collected from the pouch cell and washed with anhydrous methanol to remove the residual $AlCl_3$/EMIC ionic liquid electrolyte. The as-rinsed graphitic foams were attached to a Si wafer and baked at 90 °C for 10 min to remove residual methanol. The samples were sealed in a plastic pouch to avoid contamination by reaction with moisture and oxygen before XPS and AES characterization. Auger electron spectra were taken by a PHI 700 Scanning Auger Nanoprobe operating at 10 kV and 10 nA. XPS spectra were collected on a PHI VersaProbe Scanning XPS Microprobe (Fig. 4 in the main text).

TGA measurements. Fully charged PG cathodes were washed with methanol for 24 h to remove the residual $AlCl_3$/EMIC ionic liquid electrolyte. The as-washed PG samples were calcined at 850 °C for 3 h in air. The as-calcined samples (white foam) were collected, weighed, and analysed by SEM-EDX to study the chemical composition (Extended Data Fig. 10c). SEM and SEM-EDX analyses were performed using an FEI XL30 Sirion scanning electron microscope.

Sample size. No statistical methods were used to predetermine sample size.

21. Zhang, B. *et al.* Plasmonic micro-beads for fluorescence enhanced, multiplexed protein detection with flow cytometry. *Chem. Sci.* **5,** 4070–4075 (2014).
22. Tabakman, S. M., Chen, Z., Casalongue, H. S., Wang, H. & Dai, H. A new approach to solution-phase gold seeding for SERS substrates. *Small* **7,** 499–505 (2011).
23. Lee, J. J., Bae, I. T., Scherson, D. A., Miller, B. & Wheeler, K. A. Underpotential deposition of aluminum and alloy formation on polycrystalline gold electrodes from $AlCl_3$/EMIC room-temperature molten salts. *J. Electrochem. Soc.* **147,** 562–566 (2000).
24. Pan, S.-J., Tsai, W.-T., Chang, J.-K. & Sun, I. W. Co-deposition of Al–Zn on AZ91D magnesium alloy in $AlCl_3$–1-ethyl-3-methylimidazolium chloride ionic liquid. *Electrochim. Acta* **55,** 2158–2162 (2010).
25. Endres, F., MacFarlane, D. & Abbott, A. *Electrodeposition from Ionic Liquids* (Wiley & Sons, 2008).
26. Carlin, R. T., De Long, H. C., Fuller, J. & Trulove, P. C. Dual intercalating molten electrolyte batteries. *J. Electrochem. Soc.* **141,** L73–L76 (1994).
27. Bao, W. *et al.* Approaching the limits of transparency and conductivity in graphitic materials through lithium intercalation. *Nature Commun.* **5,** 4224 (2014).
28. Zhang, X., Sukpirom, N. & Lerner, M. M. Graphite intercalation of bis(trifluoromethanesulfonyl) imide and other anions with perfluoroalkanesulfonyl substituents. *Mater. Res. Bull.* **34,** 363–372 (1999).
29. Özmen-Monkul, B. & Lerner, M. M. The first graphite intercalation compounds containing tris(pentafluoroethyl)trifluorophosphate. *Carbon* **48,** 3205–3210 (2010).

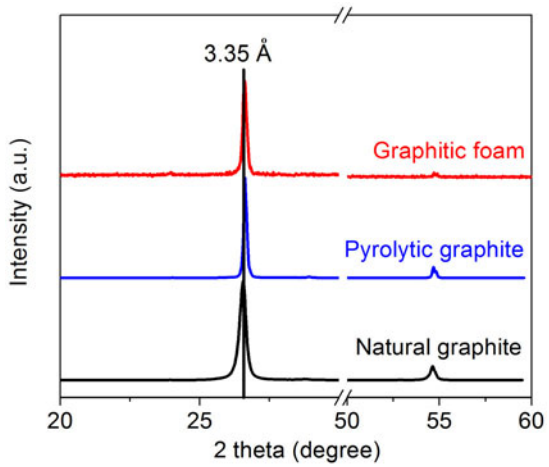

Extended Data Figure 1 | X-ray diffraction patterns of graphitic cathode materials. The natural graphite, pyrolytic graphite (PG) and graphitic foam exhibited typical graphite structure, with a sharp (002) X-ray diffraction (XRD) graphite peak at $2\theta \approx 26.55^{\circ}$ (d spacing = 3.35 Å).

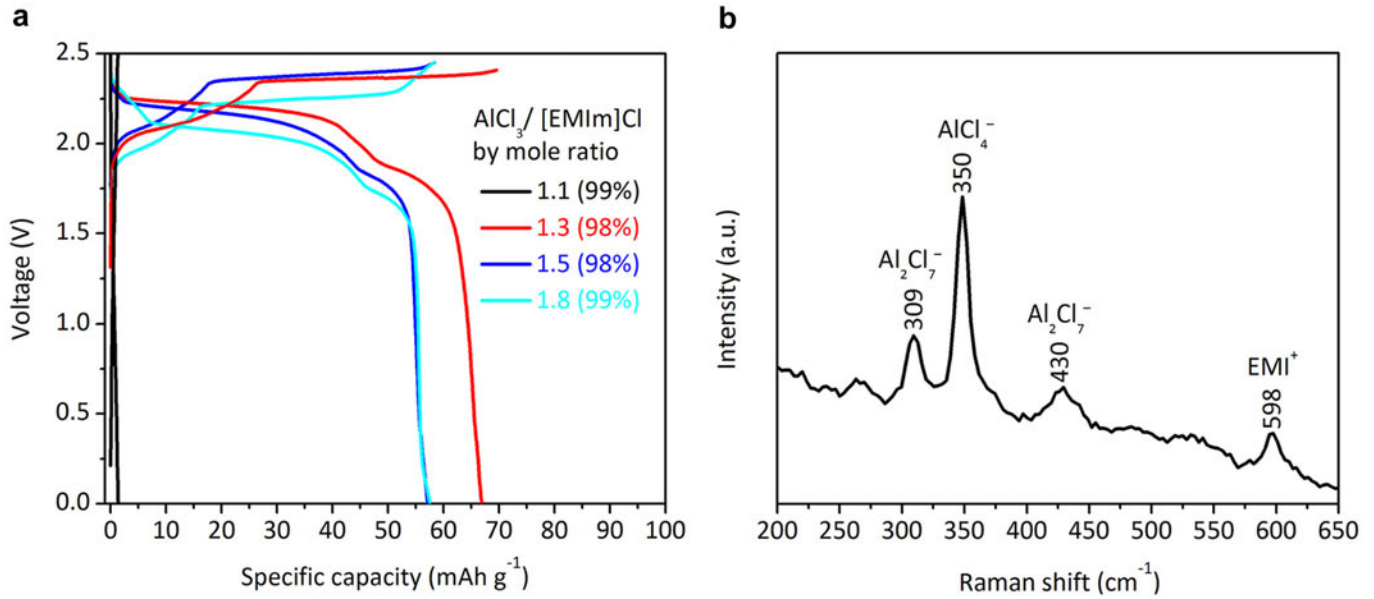

Extended Data Figure 2 | Determination of the optimal mole ratio of $AlCl_3$/[EMIm]Cl ionic liquid electrolyte. **a**, Galvanostatic charge and discharge curves of Al/PG cells at a current density of 66 mA g^{-1} in various mole ratios (1.1, 1.3, 1.5 and 1.8) of $AlCl_3$/[EMIm]Cl ionic liquid electrolytes in a Swagelok-type cell. The Coulombic efficiencies of the cells are shown in parentheses. **b**, Raman spectrum of the ionic liquid electrolyte with a mole ratio of $AlCl_3$/[EMIm]Cl = 1.3.

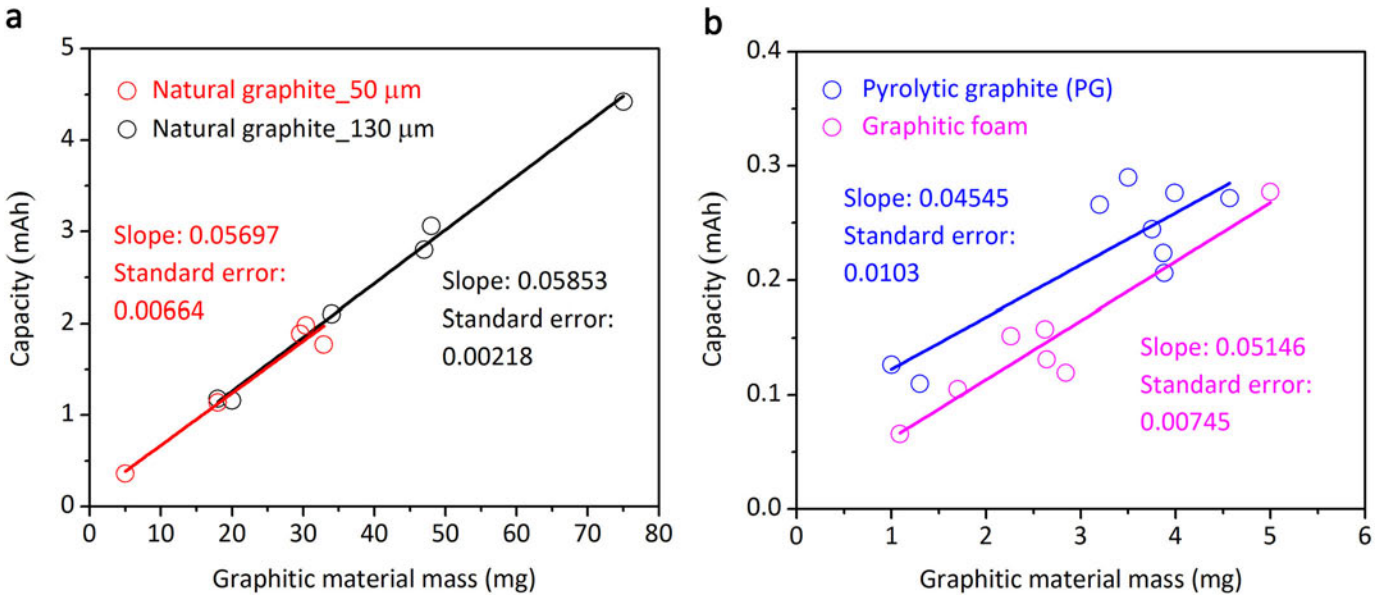

Extended Data Figure 3 | Calculated discharging capacities of Al/graphite cells with different masses of graphitic materials. **a**, Natural graphite foils of 50 μm and 130 μm thickness; **b**, PG and graphitic foam. These data suggest that the entire graphitic material (natural graphite, PG and graphitic foam) participated in the cell cathode reaction.

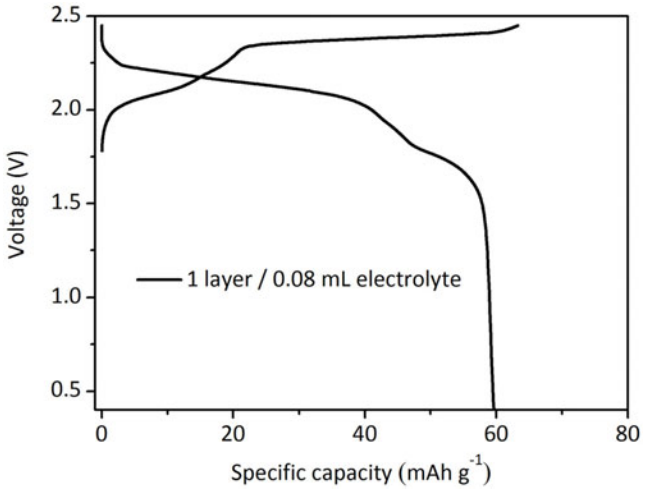

Extended Data Figure 4 | Galvanostatic charge and discharge curves of an Al/PG cell. The cell was constructed with one layer of glass fibre separator and 0.08 ml of ionic liquid electrolyte, suggesting that the minimum amount of electrolyte could be 0.02 ml per mg of PG. This electrochemical study was performed in an ionic liquid electrolyte of composition $AlCl_3$/[EMIm]Cl = 1.3 (by mole) at a current density of 66 mA g^{-1} in a Swagelok-type cell.

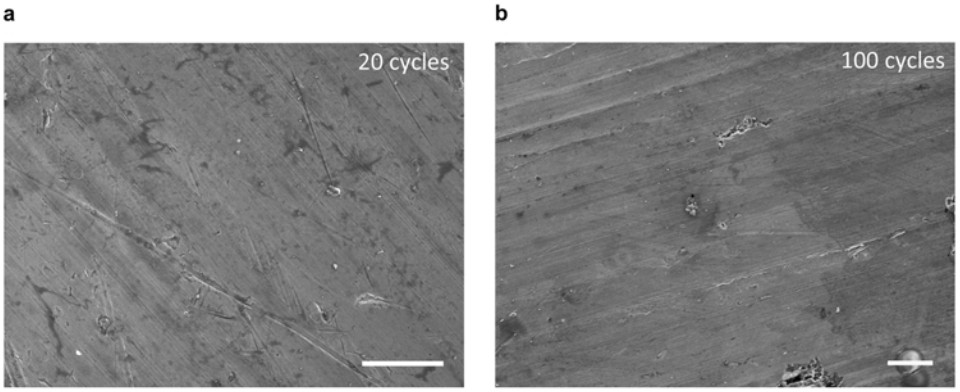

Extended Data Figure 5 | Surface observations of an Al anode. **a**, **b**, SEM images of the Al anode obtained from two Al/PG cells after 20 (**a**) and 100 (**b**) cycles, respectively, and indicate no dendrite formation over these cycles. Scale bars, 10 μm.

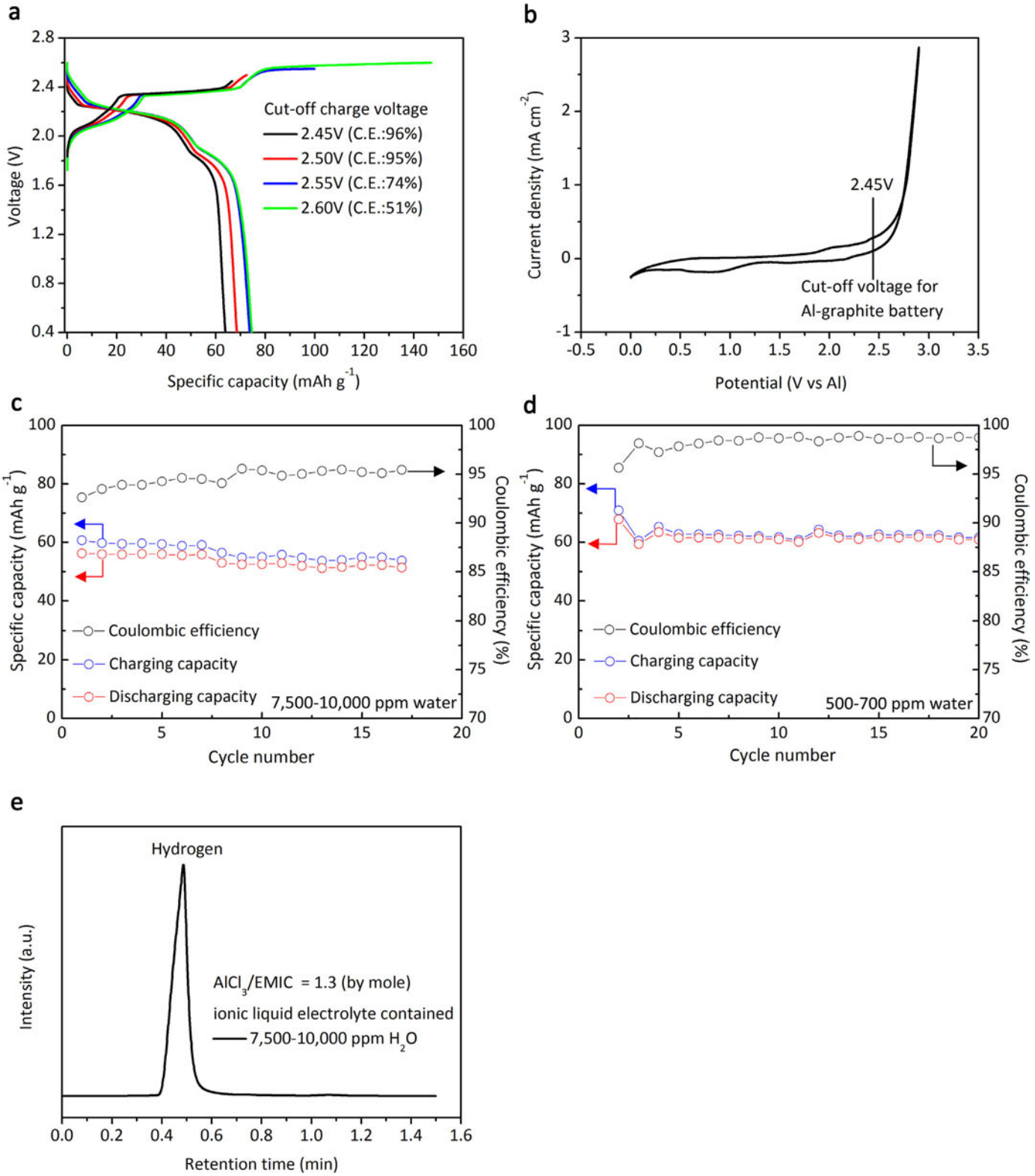

Extended Data Figure 6 | Electrochemical stability of the $AlCl_3$/[EMIm]Cl ionic liquid electrolyte. **a**, Galvanostatic curves of Al/PG cells with different cut-off charge voltages obtained at 66 mA g^{-1} in a Swagelok-type cell. **b**, Cyclic voltammetry curve of a Al/glassy carbon (GC) cell at 10 mV s^{-1} in a Swagelok-type cell. **c**, **d**, Stability test of Al/natural graphite pouch cell at 66 mA g^{-1} in electrolytes containing water at 7,500–10,000 p.p.m. (**c**) and 500–700 p.p.m. (**d**). The Coulombic efficiencies are respectively 95.2% and 98.6%, and the discharge capacities are respectively 54.9 and 61.8 mA h g^{-1} at the 15 cycle. **e**, Gas chromatography spectrum of gaseous samples withdrawn from Al/graphite cells after 30 cycles using electrolyte with 7,500–10,000 p.p.m. H_2O content. The peak found in the retention time at ~0.5 min corresponds to hydrogen gas and matches the retention time of pure hydrogen gas used for calibration.

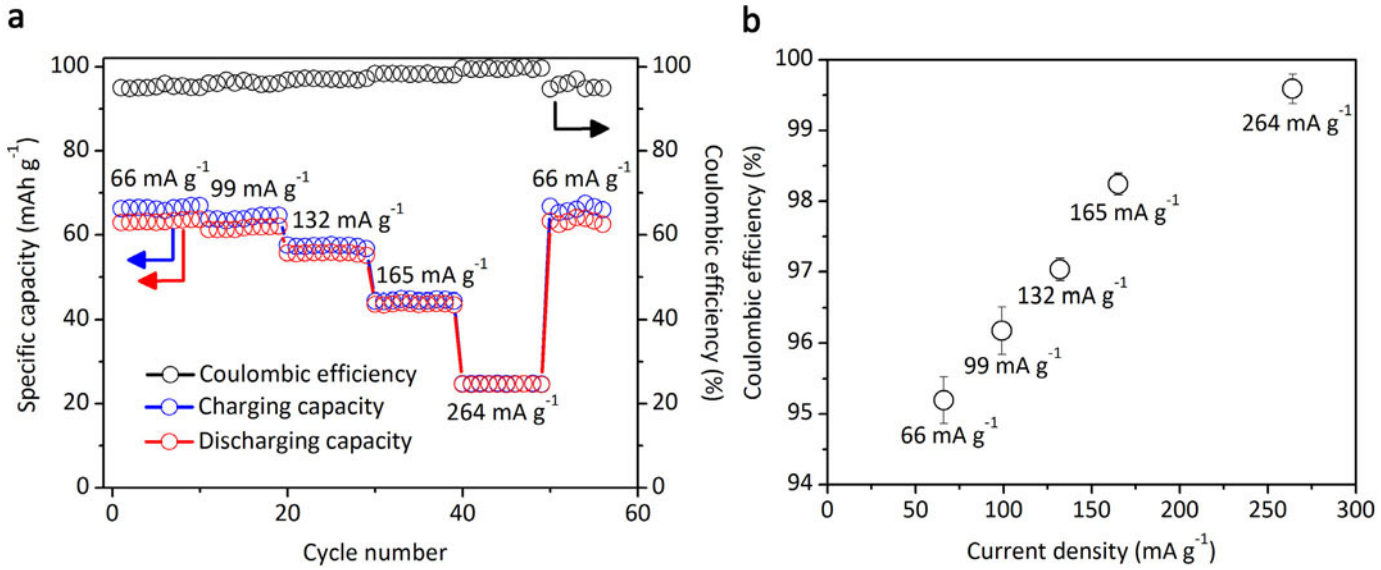

Extended Data Figure 7 | Rate capability of an Al/PG cell. **a**, Capacity retention of an Al/PG cell cycled at various current densities, showing good cycling stability at different charge–discharge current densities. **b**, Coulombic efficiency versus current density data of Al/PG cells, indicating the Coulombic efficiency is ~95–97% at current densities of 66–132 mA g^{-1}. Error bars, standard deviation from the Coulombic efficiency for each current density. All electrochemical studies were performed in an ionic liquid electrolyte of composition $AlCl_3$/[EMIm]Cl = 1.3 (by mole) in a Swagelok-type cell.

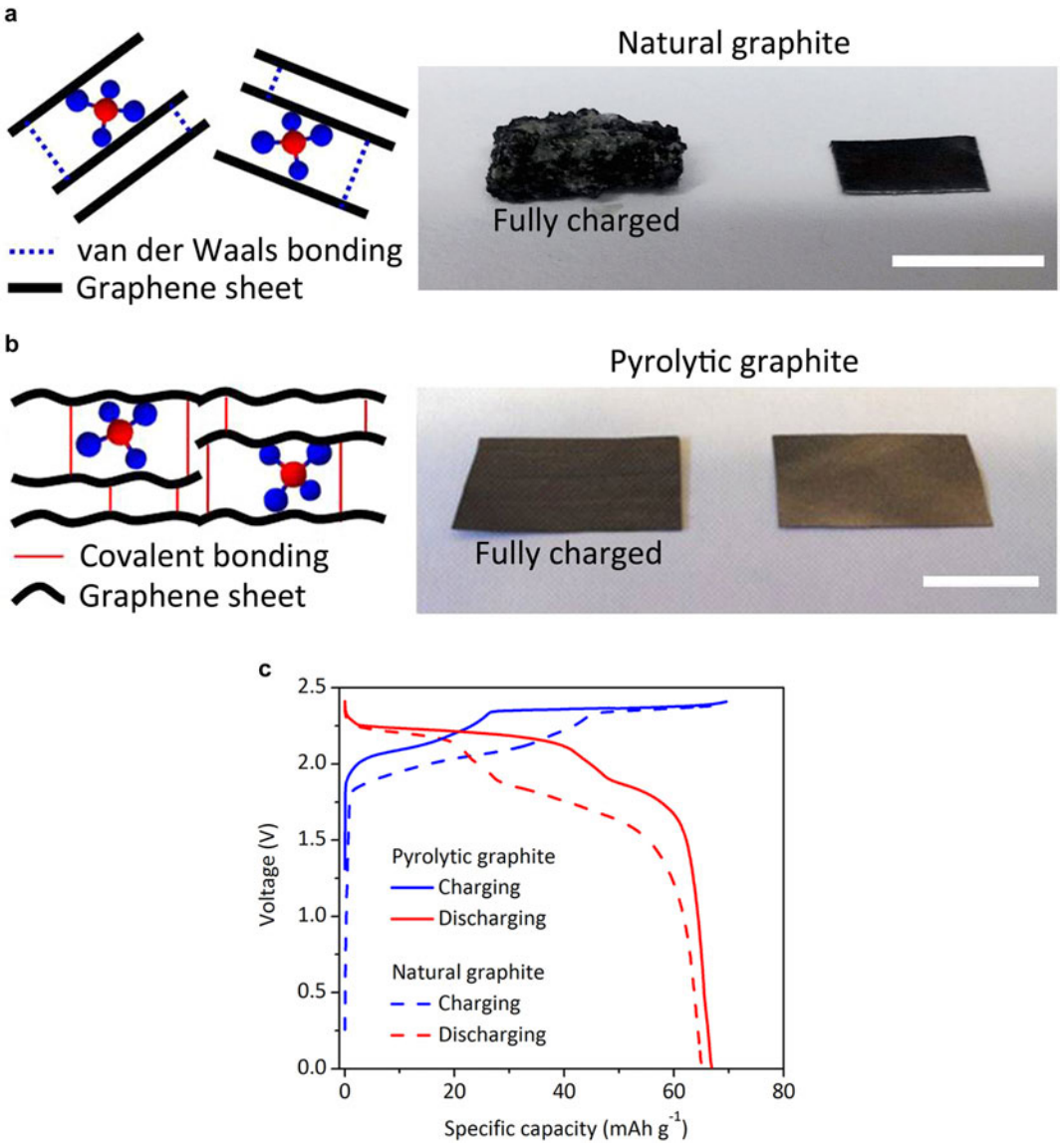

Extended Data Figure 8 | Advantages of PG as the cathode for an Al/graphite cell. **a**, **b**, Right: photographs of natural graphite (**a**) and pyrolytic graphite (PG; **b**) before and after being fully charged in an $AlCl_3$/[EMIm]Cl = 1.3 (by mole) ionic liquid electrolyte. Scale bars, 1 cm. Left: the schematic plots indicate the chemical bonds between the graphene sheets of natural graphite (Vander Waals bonding) and of PG (covalent bonding). **c**, Galvanostatic charge and discharge curves of an Al/PG cell (at 66 mA g^{-1}) and an Al/natural graphite cell (at 33 mA g^{-1}) in an ionic liquid electrolyte of composition $AlCl_3$/[EMIm]Cl = 1.3 (by mole) in a Swagelok-type cell.

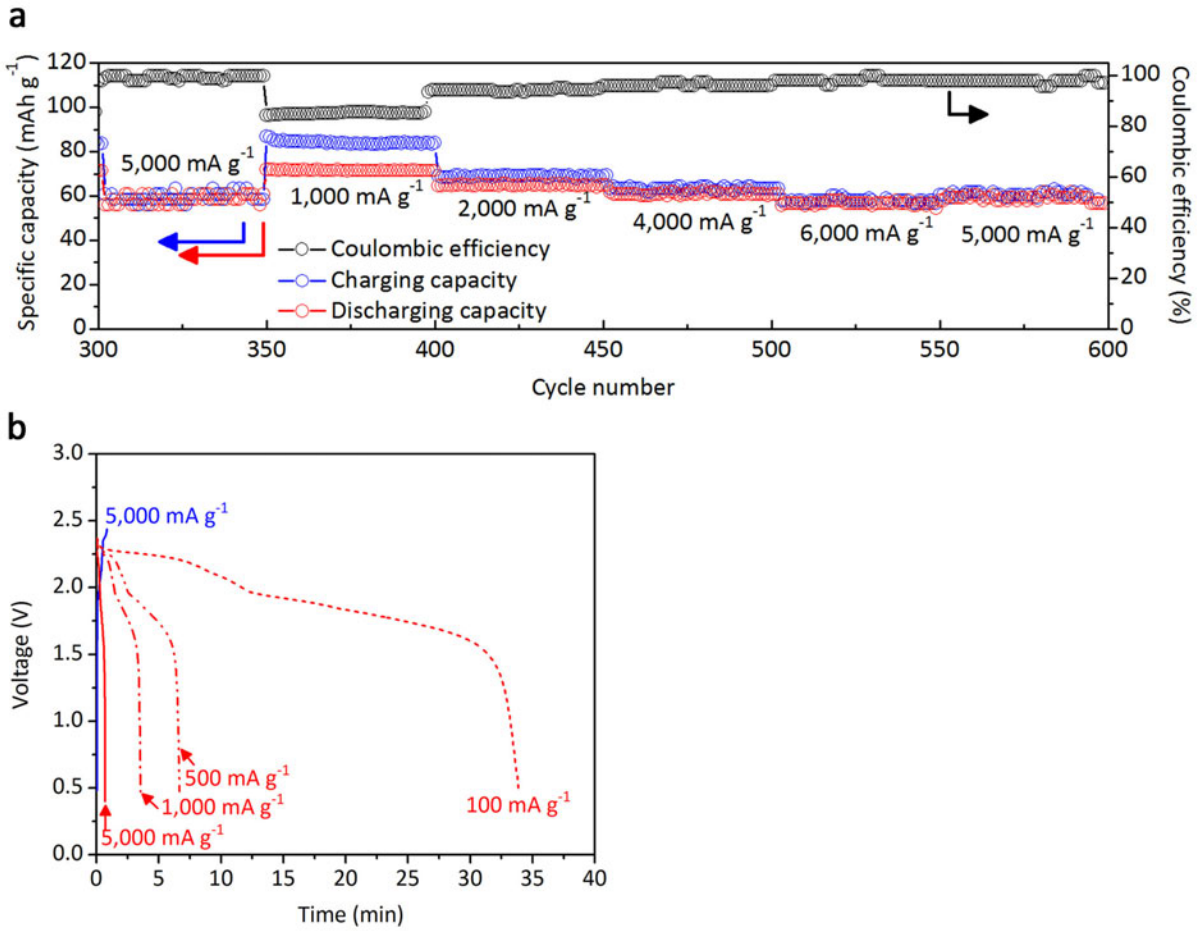

Extended Data Figure 9 | Rate capability of an Al/graphitic-foam cell. **a**, Capacity retention of an Al/graphitic-foam cell cycled at various current densities, showing cycling stability at different charge–discharge current densities. All electrochemical studies were performed in an $AlCl_3$/[EMIm]Cl = 1.3 (by mole) ionic liquid electrolyte in a pouch cell. **b**, Galvanostatic charge and discharge curves of Al/graphitic-foam cells charging at 5,000 mA g^{-1} and discharging at various current densities ranging from 100 to 5,000 mA g^{-1}. Same electrolyte and cell type as **a**.

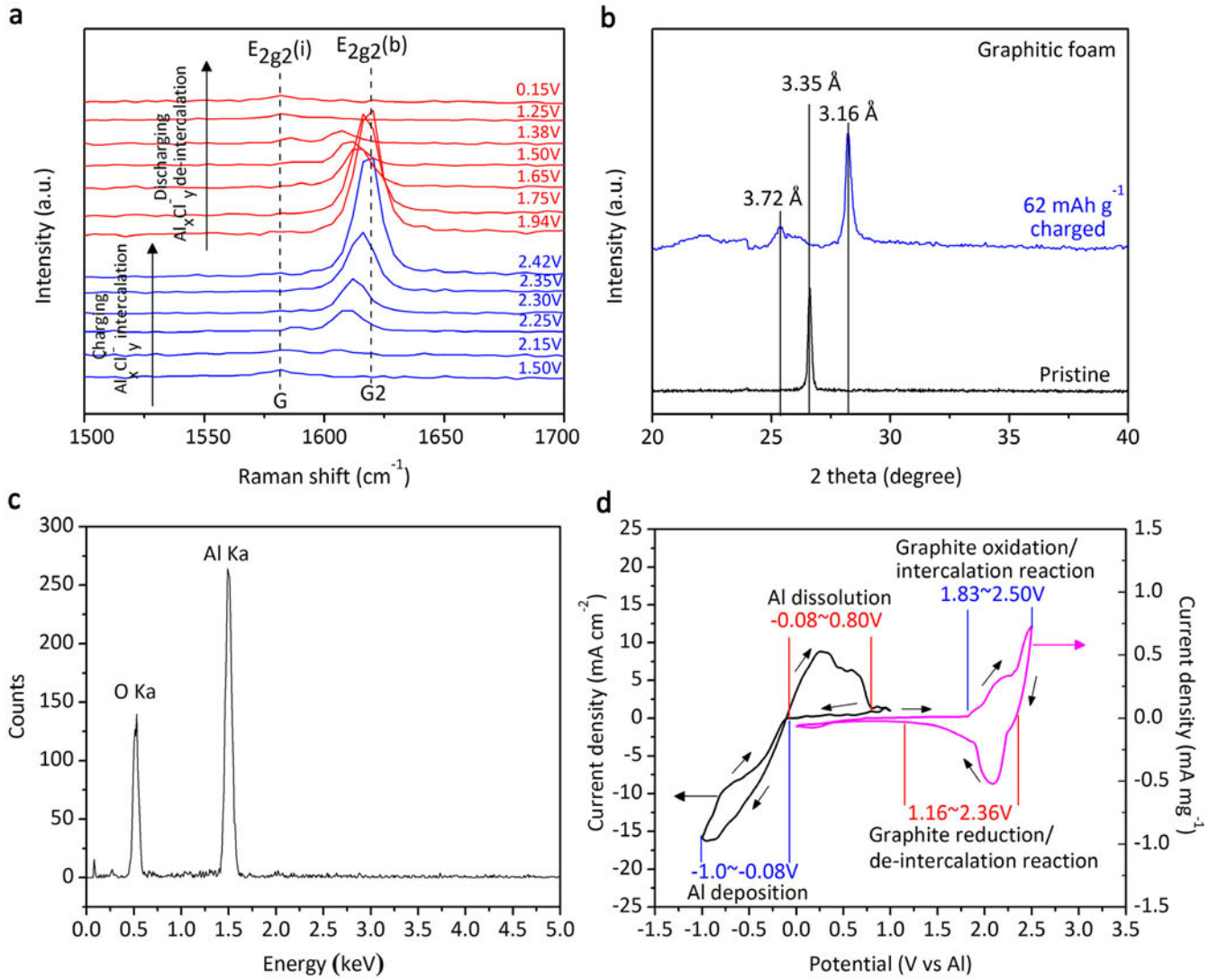

Extended Data Figure 10 | Reaction mechanism of graphitic cathodes. **a**, *In situ* Raman spectra recorded for the graphitic-foam cathode through a charge/discharge cycle showing chloroaluminate anion intercalation/de-intercalation into graphite. **b**, *Ex situ* XRD patterns of the pristine and fully charged (62 mA h g^{-1}) graphitic foam. **c**, EDS spectrum of as-calcined fully charged (62 mA h g^{-1}) PG at 850 °C in air. **d**, Cyclic voltammetry curves of Al foil and PG at a scan rate of 10 mV s^{-1} against an Al reference electrode.